Structure and Function of the Horn Shark (*Heterodontus francisci*) Cranium Through Ontogeny: Development of a Hard Prey Specialist

Adam P. Summers,[1]* Richard A. Ketcham,[2] and Timothy Rowe[2]

[1]*Ecology and Evolutionary Biology, University of California, Irvine, California 92697*
[2]*Department of Geological Sciences, The University of Texas at Austin, Austin, Texas 78712*

ABSTRACT The horn sharks (Heterodontidae: Chondrichthyes) represent one of four independent evolutions of durophagy in the cartilaginous fishes. We used high-resolution computed tomography (CT scanning) to visualize and quantify the mineralized tissue of an ontogenetic series of horn sharks. CT scanning of neonatal through adult California horn sharks (*Heterodontus francisci*) confirmed that this technique is effective for examining mineralized tissue in even small (<10 mm) specimens. The jaw joint is among the first areas to become mineralized and is the most heavily mineralized area in the cranium of a neonatal horn shark. The hyoid is also well mineralized, although the poorly mineralized molariform teeth indicate that the neonatal animal may be a suction feeder on softer prey. The symphysis of the jaws never mineralizes, in sharp contrast to the condition in the hard prey-crushing stingrays. Digitally reslicing the CT scans along the jaws allowed measurement of the second moment of area (I_{na}). Assuming that the jaws are made of the same material at all ages, I_{na} is an indicator of the flexural stiffness of the jaws. In all sizes of shark the lower jaws were stiffer than the upper and the stiffness increased in the area of the molariform teeth. The central region of the jaws, where the rami meet, support cuspidate grasping teeth and has the lowest I_{na}. The spotted eagle ray (*Aetobatus narinari*), a hard prey-crushing stingray, shows a different pattern of flexural stiffness, with the peak at the central part of the jaws where the prey is reduced between flattened tooth plates. Although the eagle ray jaws have a higher I_{na} than the horn shark, they are also far more heavily mineralized. When the relative amounts of mineralization are taken into account, horn sharks do better with what mineral they have than does the eagle ray. With a tight jaw joint and loose mandibular symphysis, as well as nearly opposite patterns of stiffness in the jaws, it is clear that two of the clades of hard prey specialists use very different methods for cracking the hard prey problem. J. Morphol. 260:1–12, 2004.

KEY WORDS: CT scan; second moment of area; durophagy; eagle ray; *Aetobatus narinari*

The cartilaginous fishes (Chondrichthyes), or ratfish, sharks, and rays, are a monophyletic, ancient assemblage of species found in all the oceans of the world, inhabiting a very broad range of ecological niches. In spite of, or perhaps because of, their skeletal material they are capable of performing at functional extremes — extant sharks are the largest fishes ever to swim in the oceans (Gudger, 1941), fast-swimming piscivorous species can likely move as rapidly as even the fastest bony fishes (Fierstine and Walters, 1968; Compagno, 1984), and certain species are able to exert sufficient force with their cartilaginous jaws to crush mollusks (Coles, 1910; Summers, 2000). In the several radiations of cartilaginous fishes that have adopted a durophagous diet there are likely multiple solutions to the problem posed by orally crushing prey that is harder than the skeleton of the jaws.

Previous studies have examined the mechanics and morphology of hard prey-crushing in the myliobatid stingrays (Summers et al., 1998; Summers, 2000), one of four independent acquisitions of a durophagous diet in the chondrichthians (Fig. 1). The ten species of horn sharks (Heterodontiformes:Heterodontidae) also crush hard prey between molariform oral jaw teeth, although these teeth are not nearly as specialized as those of the stingrays (Smith, 1942; Nobiling, 1977; Segura-Zarzosa et al., 1997). As their name implies, the genus *Heterodontus* is characterized by having more than one tooth shape — multicuspidate anterior teeth suited for grasping, and rounded, broad molariform teeth for crushing. Both types of teeth are present by the time the neonate shark hatches from its egg case (Garman, 1913; Smith, 1942). Examinations of the feeding mechanism of durophagous sharks have focused on muscular anatomy (Nobiling, 1977) and the kinematics of feeding (Wilga and Motta, 2000; Edmonds

Contract grant sponsors: the McDowell Foundation (to APS), the National Science Foundation; Contract grant number: IIS-9874781 (to TR and RK).

*Correspondence to: Adam P. Summers, Ecology and Evolutionary Biology, University of California, Irvine, CA 92697.
E-mail: asummers@uci.edu

DOI: 10.1002/jmor.10141

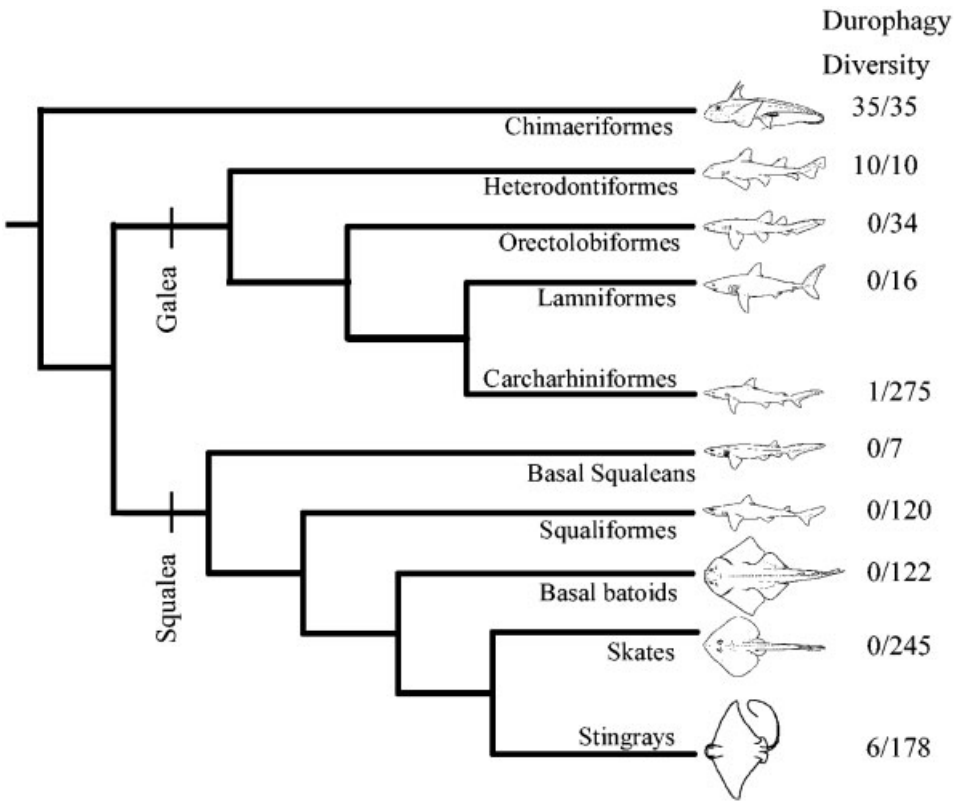

Fig. 1. Cladogram of the cartilaginous fishes showing diversity of hard prey-crushing taxa and their relationship to other cartilaginous fishes. The number of durophagous species / number of species in the clade is shown to the right. The horn sharks (Heterodontiformes) are the primary focus of this study, with some comparative data from a durophagous stingray. The topology of the cladogram is from Shirai (1996) with some clades collapsed for simplicity.

et al., 2001), but there has been no examination of the skeletal structure that allows this unusual behavior.

Cartilaginous fishes split from the lineage that gave rise to bony fishes (and tetrapods) over 320 million years ago and experienced a significant Paleozoic radiation represented today by two clades of Mesozoic origin — the chimeras and the elasmobranchs (Lund and Grogan, 1997; Coates and Sequeira, 2001). The completely cartilaginous skeleton of Recent chondrichthian fishes reflects the loss of a bony skeleton. The outgroup, placoderms, represent the plesiomorphic condition, with normal dermal bone, and there is clear evidence that some fossil sharks had structurally significant endoskeletal bone (Halstead, 1974; Smith and Hall, 1990; Coates et al., 1998). Extant chondrichthians have abandoned endoskeletal bone in favor of a cartilaginous skeleton that is mineralized to varying degrees (Ørvig, 1951; Applegate, 1967; Kemp and Westrin, 1979).

The mineralization of the shark endoskeleton, composed of calcium phosphate hydroxyapatite, takes several forms — the web-like calcified structures of the vertebrae (aereolar mineralization); the prismatically mineralized crystals on the outer surface of skeletal elements; and a less dense, globular calcification usually associated with the prismatic material (Ridewood, 1921; Ørvig, 1951; Summers, 2000). The globular and prismatic mineralization is arranged in a series of thin, irregularly shaped tiles, called "tesserae," on the surface of the skeletal element (see Clement, 1992, for a review). The interior of these skeletal elements is composed of a hyaline, unmineralized cartilage. The mineralized tesserae are thin (~1 mm) and form one or more layers of tiles over the softer hyaline core. The mineralized shell that surrounds a skeletal element is stiffer and stronger than the underlying cartilage and, for the purposes of this article, that core is ignored. The stiffness of the skeletal element is presumed to come primarily from the tiled layer(s) of tesserae.

Three-dimensional reconstructions of mineralized tissue from computed tomography scans (CT scans) are becoming increasingly available to morphologists (Rowe, 1996; Rowe et al., 1997; Cifelli et al., 1999; Clark et al., 2002). These scans are visually engaging and provide a unique opportunity to understand the positions of skeletal elements relative to soft, less radio-opaque tissues such as unmineralized cartilage and tendon. CT scans also represent a largely untapped source of data describing the structure of skeletal elements. For example, it is possible to "virtually section" a CT reconstruction along any arbitrary axis. These sections can then be analyzed using traditional structural metrics such as second moment of area. It is now possible to extract objective, numerical descriptors of the skeleton from digitally reconstructed skeletons.

The purpose of this article is threefold: 1) to explore the capabilities of high-resolution CT scanning to assess mineralization in small (<1 cm) chondrichthyan specimens; 2) to describe the ontogeny of the mineralization of the chondrocranium, jaws, and hyoid arch elements from a series of horn sharks; and 3) to compare horn shark jaw morphology among three ontogenetic stages and another hard prey-crushing elasmobranch, the spotted eagle ray (*Aetobatus narinari*).

MATERIALS AND METHODS

Animals

Four freshly killed adult and juvenile California horn sharks (*Heterodontus francisci*) were obtained from the coastal waters of southern California through the Scripps Institute of Oceanography in La Jolla. Each animal was measured and sexed and the head and branchial arches were removed from the largest (AL21, TL 58.5 cm, female) and smallest (AL22, 38 cm, female) animals and frozen for CT scanning. The other two animals were dissected while fresh to ascertain the positions of jaw muscles, the mobility of the symphyseal joint, and the mobility of the hyomandibulae. A neonatal California horn shark (P1999, 12.5 cm, male), hatched in captivity at the University of California, Santa Barbara, was preserved in formalin and stored in 70% ETOH. This animal was used whole for the CT scanning process.

Fresh-frozen heads of the spotted eagle ray, *Aetobatus narinari*, were obtained from commercial fisherman in Puerto Rico. For this study a set of jaws was dissected from a 1.8-m disk-width adult male animal, preserved in formalin, then stored in ETOH for CT scanning.

CT Scanning

The specimens were scanned at the High-Resolution X-ray Computed Tomography (CT) Facility at the University of Texas at Austin, which is described by Ketcham and Carlson (2001). For the scans of *Aetobatus narinari* and the adult horn shark (AL21), the high-resolution subsystem was used. Both scans utilized X-ray settings of 420 kV and 1.8 mA, with a focal spot size of 0.8 mm. X-ray intensities were measured using an RLS detector with 2048 channels spaced at 0.05-mm intervals and the X-ray beam was collimated to achieve 0.25-mm-thick slices. A series of slices spaced at 0.25 mm was acquired for each, with reconstruction parameters calibrated to maximize usage of the 12-bit range of grayscales available in the output images.

For the *Aetobatus narinari*, the X-rays were prefiltered to reduce beam-hardening artifacts using a 1.5875-mm-thick brass plate. Each slice was acquired using 2,000 views (angular orientations), each view having an acquisition time of 64 ms, and detector gain was set to 4 to maximize count rate, resulting in a net scan time of ~130 sec per slice. Detector readings were averaged in sets of four to reduce noise and speed reconstruction of 1024 × 1024 images. The sample was scanned in 190% offset mode, in which the sample is placed off-center in the X-ray fan beam (Ketcham and Carlson, 2001), permitting a field of view of 133 mm. The jaws were placed in a cylinder on top of ETOH-soaked cheesecloth, with additional damp cheesecloth draped over.

For AL21, no beam filtration was employed and images were acquired based on 1,000 views, with an acquisition time of 64 ms and a gain of 4, for a scan time of ~66 sec per slice. Detector readings were averaged in sets of two and subsequently a 5-width running average was employed on the detector data to reduce image noise. The sample was scanned in 160% offset mode, with a field of view of 105 mm.

The juvenile horn shark (AL22) and the neonate (P1999) were scanned on the ultra-high-resolution subsystem. Both scans utilized the microfocal X-ray source with settings 120 kV and 0.2 mA. Neither scan used beam filtration and both employed 160% offset mode. X-ray intensities were measured using an image intensifier connected to a 512 × 512 CCD video camera. Both specimens were scanned in 3-slice mode, in which data for three slices are acquired simultaneously. Images for AL22 were acquired with 1200 66.7 ms views per 3-slice acquisition, for a scan time of ~28 sec per image. The slice thickness and interslice spacing was 0.151 mm and the field of view was 64 mm. P1999 was scanned using 1,800 66.7 ms views per 3-slice acquisition, for a scan time of ~41 sec per image. Slice thickness and interslice spacing were both 0.0698 mm and the field of view was 28 mm.

The CT scan slices were processed with VoxBlast (VayTek Software, Fairfield, IA), which allows reconstruction of the three-dimensional structure of the shark cranium. The cranium was virtually resliced in the sagittal, coronal, and frontal planes and movies of rotations and slicings of each specimen were generated. Slices and movies of rotations are available on-line at www.digimorph.org.

Second Moment of Area

The second, or area moment of inertia (I_{na}), is a measure of how well the cross section of a beam will resist bending. Deflection (δ) in an isotropic, homogenous beam is proportional to the modulus of elasticity (E) times the second moment of area:

$$\delta \propto E\, I_{na}, \tag{1}$$

and

$$I_{na} = \int x_{na}^2\, dA \tag{2}$$

where x_{na} is the distance between the infinitesimal area dA and the neutral axis (Wainwright et al., 1976; Beer and Johnston, 1977). The neutral axis is a line perpendicular to the line of applied force that passes through the centroid of the cross section.

Before the second moment can be computed, cross sections of the beam, in this case the upper or lower jaw, must be taken perpendicular to the long axis. Our sections were generated through the CT scanning process and originally took the form of a series of slices along the arbitrary axis at which the specimen is placed in the scanner. These slices were composited into a 3D image and then virtually resliced along a straight line through the right jaw (Fig. 2). The jaws of *Heterodontus* and *Aetobatus* are nearly straight, although for curved jaws the reslicing could have been made along an arc.

A MatLab program (MathWorks, Natick, MA) was written to perform the calculations of second moment from these slices. A threshold for converting the grayscale sections (255 gray values) to black and white (bitmapped) images was determined by trial and error. Too low a threshold caused unacceptable agglomeration of calcified elements (i.e., teeth blended into jaw) and too high a threshold caused calcified elements to break into disconnected units. Setting the threshold is absolutely a subjective task and has a profound affect on the measured results (discussion of variation in threshold). There was a very narrow range of thresholds that were judged to accurately reflect the mineralization pattern — in the most difficult to judge cases the span was 8 grayscale units.

The centroid of the jaw cross section was calculated from the bitmap and the expected line of force was input. For an arbitrary skeletal element the line of force is a subjective measure, although for these jaws the occlusal surfaces of the teeth provided a simple and accurate way to estimate the direction (Fig. 2). The neutral axis was calculated and then the distance of each pixel

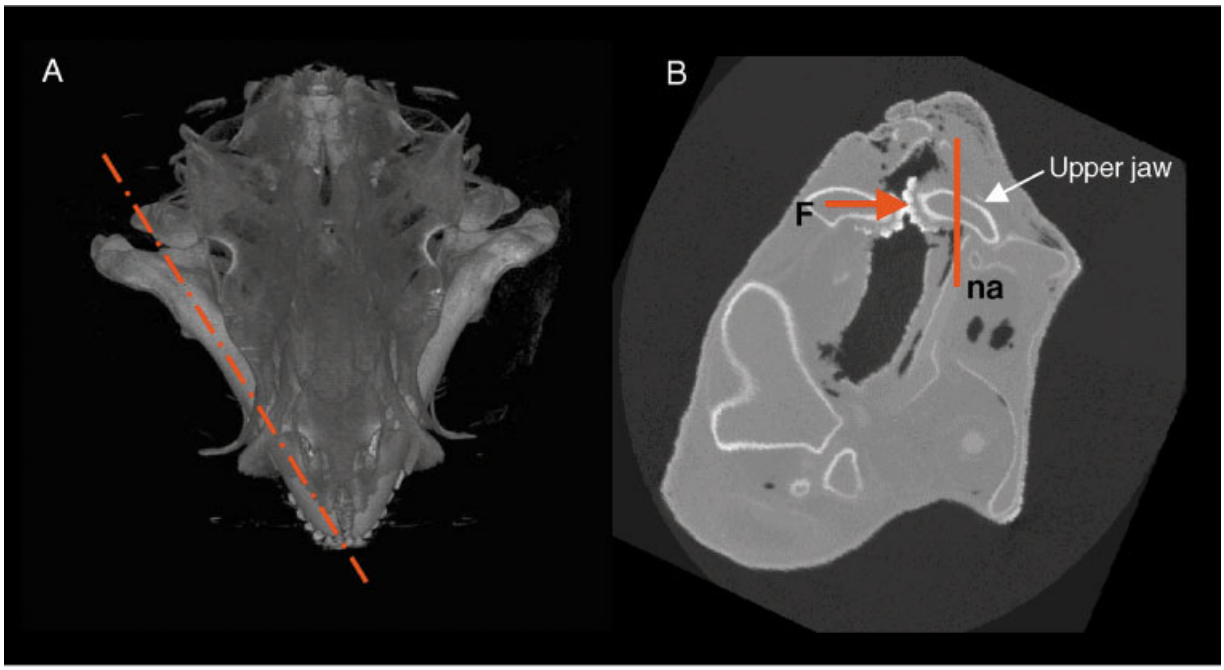

Fig. 2. **A:** Dorsal view of a horn shark (*Heterodontus francisci*) chondrocranium showing the line along which "virtual sections" are generated for calculation of second moment of area. **B:** An example section along the line in **A** has been rotated so that the neutral axis (na) is vertical. The teeth give a clear indication of the expected direction of force generation (F). The vertical red line is the neutral axis. Second moment is calculated by finding the distance between the neutral axis and each pixel in the upper jaw with a grayscale value judged bright enough to represent mineral.

from the neutral axis was squared. The second moment of the jaw cross section was calculated as the sum of these squared distances multiplied by the area in mm of a single pixel. The program for performing these operations is available at www.biomechanics.bio.uci.edu along with sample data files.

A dimensionless measure of the ability of a jaw cross section to resist bending was constructed for two reasons: 1) second moment of area is not a measure for which many people have an intuitive feel, and 2) there was a need for a measure of the extent to which available mineralized tissue is arranged to resist bending. We satisfied both requirements by taking the ratio I_{na} of the jaw to I_{na} of a circle with the same area as the jaw. This is a measure of how much better (or worse) the arrangement of mineralized tissue is than if it were simply arranged as a solid rod with circular cross section. I_{na} of a circle is given by:

$$I_{na} = \frac{\pi r^4}{4}, \tag{3}$$

where r is computed as:

$$r = \sqrt{\frac{A}{\pi}}, \tag{4}$$

where A is the area of the mineralized tissue in a particular section.

Assessing Variability in the Measurement of Second Moment

The subjective determination of the threshold for generating the black and white image from the grayscale image has the potential to significantly alter the second moment measurements. Four frames were chosen at random from the CT slices of the upper jaw of the adult horn shark. The centroid and neutral axis were determined for each frame and then the second moment was computed for thresholds ranging from 130–180.

RESULTS

Ontogeny of the Horn Shark Cranium

Although the anatomy of the chondrocranium and even its ontogeny have been described before, the CT scan reveals different information in that it records those regions that are mineralized, while previous work has looked at the shape of the cartilage without regard to mineralization (Parker, 1879; Garman, 1913; Smith, 1942). CT scanning successfully imaged the mineralized cranium, jaws, hyoid, and branchial elements in the adult, juvenile, and neonate horn shark. The 10-mm long cranium of the neonate is well calcified in the basal plate region, and both trabecular and parachordal cartilages have also mineralized (Fig. 3). The otic region of the chondrocranium near the articulation of the hyomandibulae is well mineralized, but the remainder of the cranium, including the optic and olfactory regions, are poorly mineralized. The dorsal edge of the palatoquadrate and the dorsal and ventral portions of Meckel's cartilage are well mineralized, but the lateral surface of both elements is mineralized poorly or not at all. The jaw joint was fully formed and in cross section revealed as the thickest region of mineralization in the head of the neonate. The cerato-

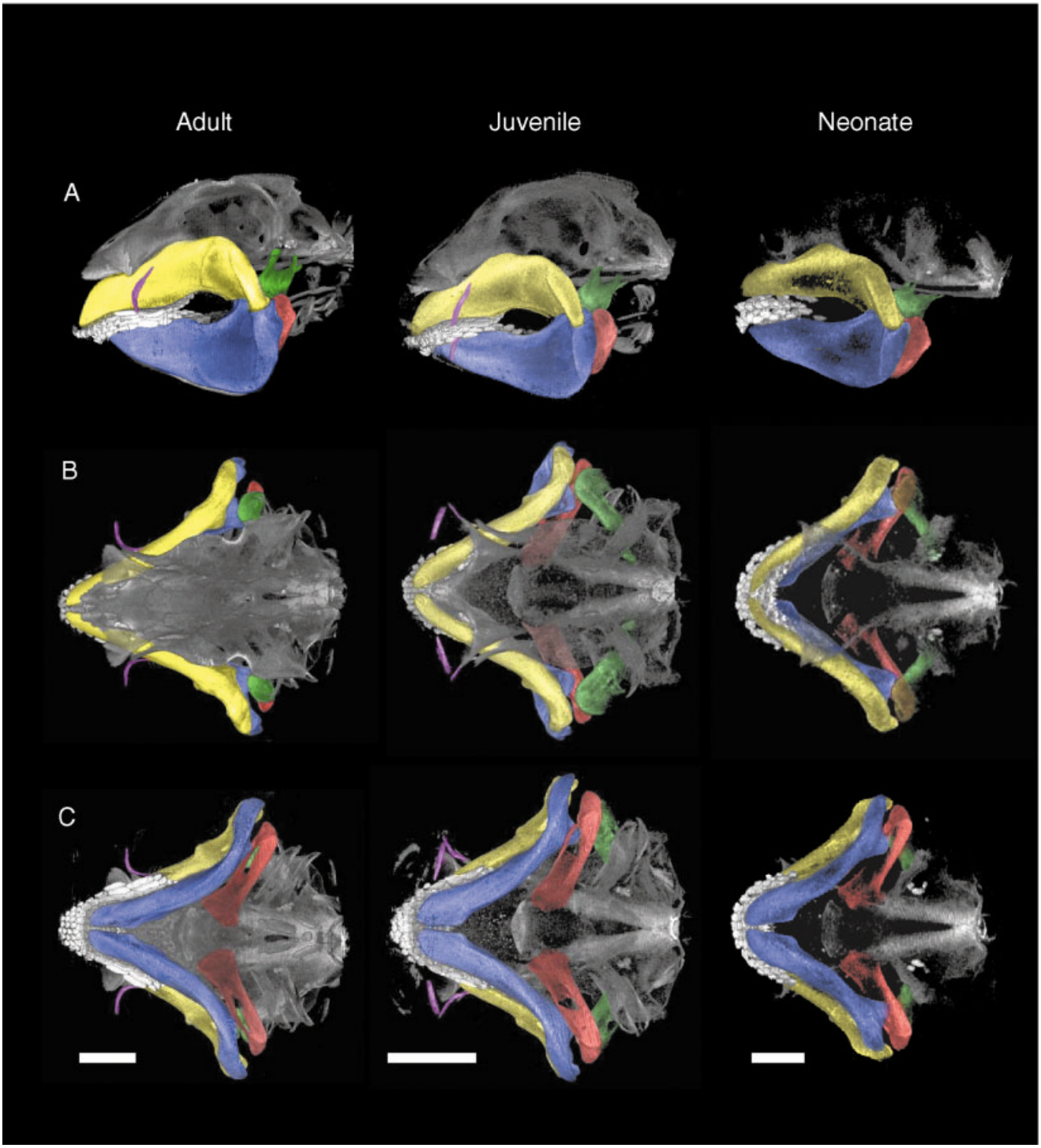

Fig. 3. Lateral (**A**), dorsal (**B**), and ventral (**C**) views of 3D reconstructions of the cranial skeleton of three ontogenetic stages of the California horn shark, *Heterodontus francisci*. The upper jaw (palatoquadrate) has been pseudocolored in yellow, the lower jaw (Meckel's cartilage) in blue. The hyomandibula (green), ceratohyal (red), and the labial cartilages (purple) are also pseudocolored. Scale bar for the adult male (58.5 cm TL) shark is 3 cm. Scale bar for the juvenile male (38 cm TL) shark is 3 cm. Scale bar for the neonate female (12.5 cm TL) shark is 2 mm.

hyal and the hyomandibulae are also well mineralized, although the latter is not as well defined as the former. The cuspidate, anterior grasping teeth are heavily mineralized and clearly visible, although the crushing teeth in the posterior of the jaw are barely mineralized. The diastema between the posterior-

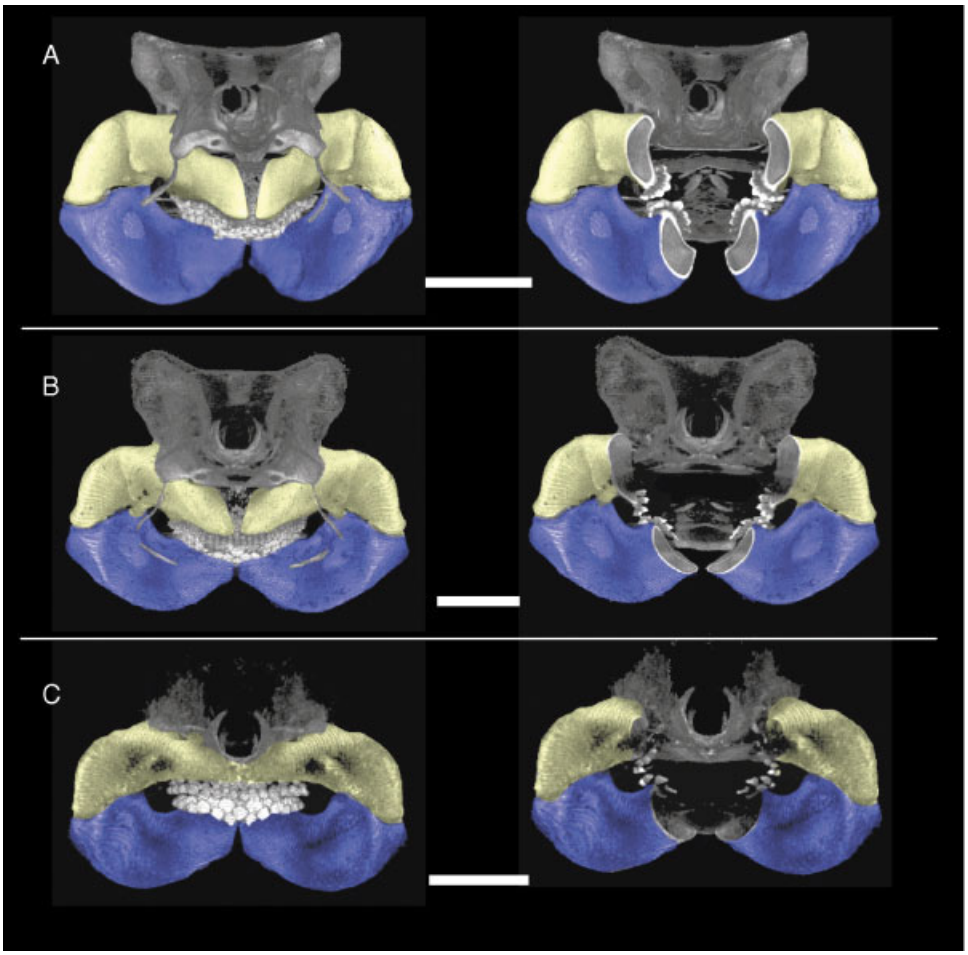

Fig. 4. Anterior views of 3D reconstructions of the cranial skeleton of the California horn shark, *Heterodontus francisci*. The upper jaw (palatoquadrate) has been pseudocolored in yellow and the lower jaw (Meckel's cartilage) in blue. The right image in each panel laterally sectioned at the level of the molariform teeth, showing the relative development of these teeth and the thickness of the mineralization in the jaws. **A:** 58.5 cm total length adult female. Scale bar = 30 mm. **B:** 38 cm total length juvenile female. Scale bar = 30 mm. **C:** 12.5 cm total length neonate male. Scale bar = 3 mm.

most teeth and the jaw joint is nearly as broad as the dentigerous portion of the jaws.

The nasal and optic regions of the chondrocranium of the juvenile horn shark are more completely mineralized than in the neonate, but the central optic and anterior nasal regions remain poorly defined. The posterior of the chondrocranium is well mineralized, but the overall shape, in lateral view, remains steeply sloping anteriorly, as in the neonate. The roof of the chondrocranium is more mineralized than in the neonate, but still appears indistinct. The dorsal and ventral labial cartilages have fully mineralized and are visible as separate elements (Fig. 3). The upper and lower jaws are fully mineralized, with the exception of a small central region in the palatoquadrate. The jaw joint is more heavily mineralized than in the neonate and the heterodont dentition is fully developed, although the molariform teeth are not as large and flat as in the adult.

In the adult the nasal cartilages are very well mineralized and serve to elongate the chondrocranium. The optic region is fully mineralized, as are the hyoid and hyomandibulae. The molariform teeth are well developed, amounting to about half of the linear dentigerous space. The jaws are fully mineralized, and as can be seen in cross section, are composed of several layers of tesserae built up to a thickness of over 1 mm (Fig. 4). The mandibular symphysis never mineralizes and dissection and manipulation reveal this joint to be exceptionally mobile even for an elasmobranch. In contrast the joint between the palatoquadrate and Meckel's cartilage articulates very tightly, has well-mineralized opposing surfaces, and allows freedom of movement only in the sagittal plane.

Anatomy of the Eagle Ray

The anatomy of the adult eagle ray jaw has been well demonstrated by several authors (Gudger, 1914; Bleeker, 1977; Summers, 2000) and, as there is little unmineralized tissue, descriptions based on dissection of cartilage are identical to the results of this study.

Second Moment of Area

In the neonatal horn shark, second moment of area increases continuously from the mesial tips of

the upper jaw to the jaw joint. The lower jaw has a higher second moment than the upper except for a small region just posterior to the molariform teeth, where they are nearly equal. At this point there is a dip in I_{na} and it remains constant or slightly declining for a few mm before rising again to the joint with the upper jaw (Fig. 5). A similar pattern is seen in the juvenile except that the rise in I_{na} of the upper jaw is also briefly interrupted just behind the molariform teeth, where it dips then continues to rise. This pattern is most extremely seen in the adult horn shark where I_{na} rises to a sharp peak in the same region. The upper jaw I_{na} decreases from this point to mid-diastema and then increases to equal the peak behind the teeth, while the second peak in the lower jaw is twice as high as the first. In all three animals the I_{na} rises more steeply in the lower jaw than in the upper. The peak second moment of the adult is an order of magnitude higher than that of the juvenile and 600 times that of the neonate.

The mineralized tissue of the jaws is arranged to resist flexion 4–35 times better than if it were a solid rod of circular cross section (Fig. 6). Across ontogeny the lower jaw increases from a maximum of 18 times better in the neonate to 35 times better in the adult. The upper jaw shows a similar increase from 8–18 times better. The profiles of the "stiffness" ratio are different from the second moment profiles in that the dip in magnitude between the molariform teeth and the jaw joint is either small or nonexistent. The juvenile and the adult are similar in magnitude, while the values for the neonate are about half those of the other two at any point along the jaws (Fig. 6).

The I_{na} of the eagle ray upper jaw peaks at the symphysis of the jaws, drops between the symphysis and the edge of the tooth plate, and then rises again to an equal peak at the lateral edge of the jaws (Fig. 7). The sharp ventral bend in the rami of the jaw just medial to the joint with the palatoquadrate meant that the sections were not perpendicular in this region, so analysis was stopped at the location indicated in Figure 7. The maximum second moment of the eagle ray jaw was eight times higher than the highest value from the adult horn shark and the minimum for the eagle ray was still over four times higher than the maximum horn shark value. However, the peak values for the ratio of I_{na}/I_{circle} were lower for the eagle ray than for the adult and juvenile horn sharks — an indication that the ray has a more mineralized jaw, while the horn shark mineralization is better arranged to resist bending (Figs. 6, 7).

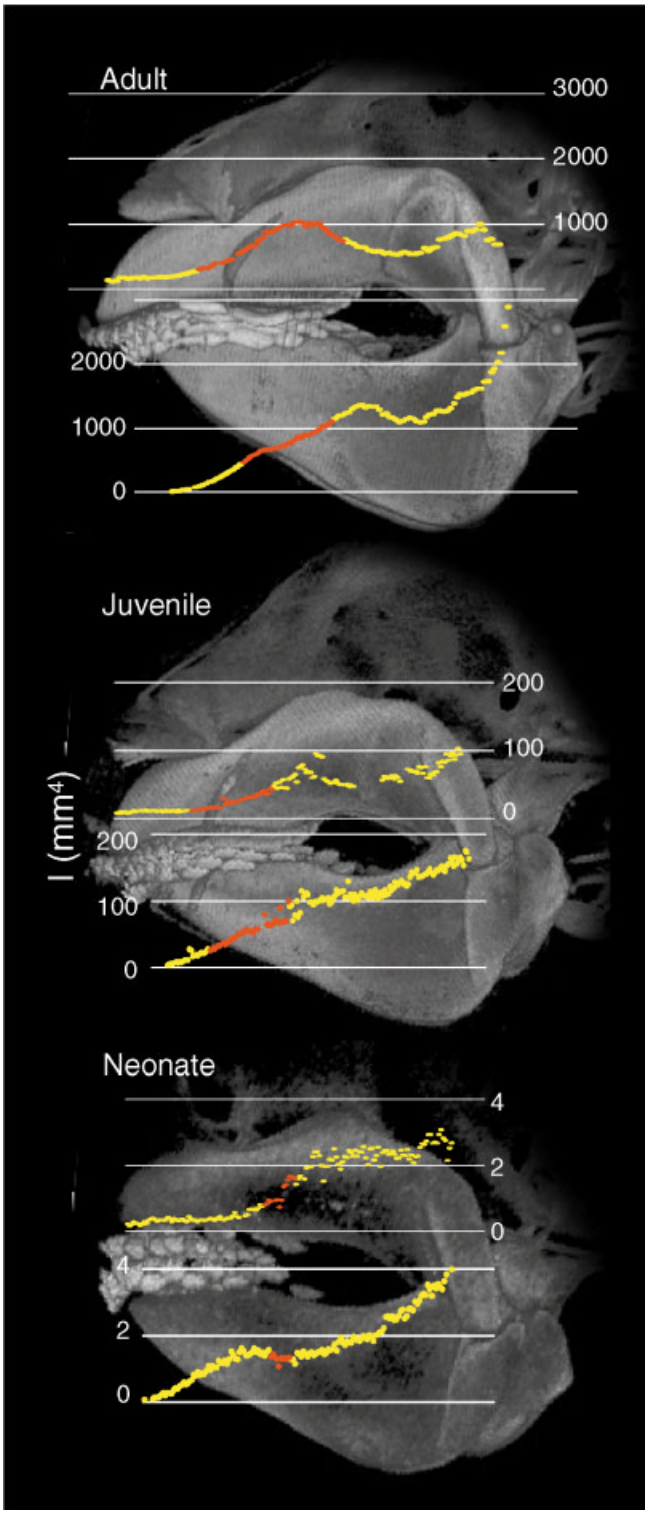

Fig. 5. Second moment of area of the cross section of the upper and lower jaws superimposed over a reconstruction of the horn shark cranium. The x-axis position of each point on the graph corresponds to the position of the section through jaws in the background. Points corresponding to sections with molariform teeth are in red. The y-axis scale varies among the adult (top), juvenile (middle), and neonate (bottom) pairs of graphs.

Variation in Second Moment Due to Threshold Changes

For all four sections, I_{na} decreased with increasing threshold. For frames 76, 139, and 100 the decrease was linear ($r^2 = 0.97–0.99$), but for section 119 there is an inflection point at a threshold of 136 that

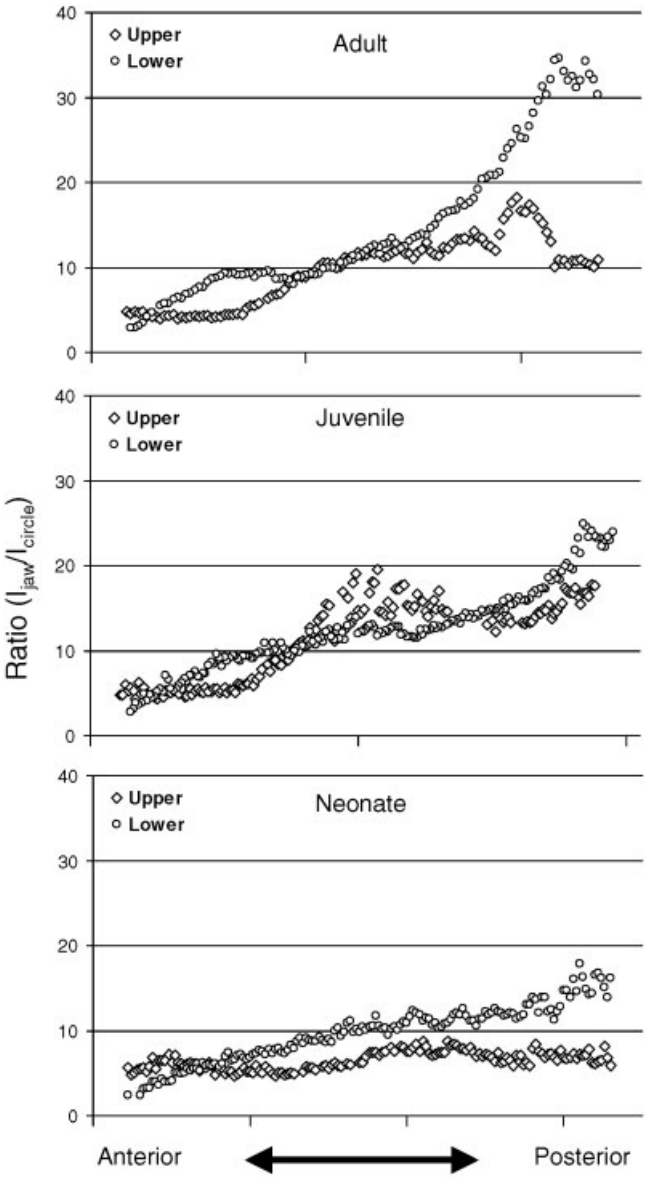

Fig. 6. The relationship between position along the jaw (anterior–posterior) and a dimensionless measure of cross sectional shape — the ratio of the second moment of area of the jaw cross section to the second moment of area of a circle with the same first moment of area. The sections run from the tips of the jaws (anterior) to the first section of the palatoquadrate-Meckel's cartilage joint.

reflects the abrupt inclusion of some of the teeth in the bitmap of the jaw (Fig. 8). Over the narrow range of thresholds that were judged to accurately reproduce mineralization patterns, I_{na} varied by $< 10\%$.

DISCUSSION

Crushing Hard Prey

The horn shark and the myliobatid stingrays have quite different equipment for crushing hard prey. The heavily calcified upper and lower jaws of the stingray, as exemplified by the spotted eagle ray and by the cownose ray (Summers, 2000), have extensive soft tissue filling a gap at the jaw joint. Neither palatoquadrate nor Meckel's cartilage has a moveable symphysis, making the left and right sides of

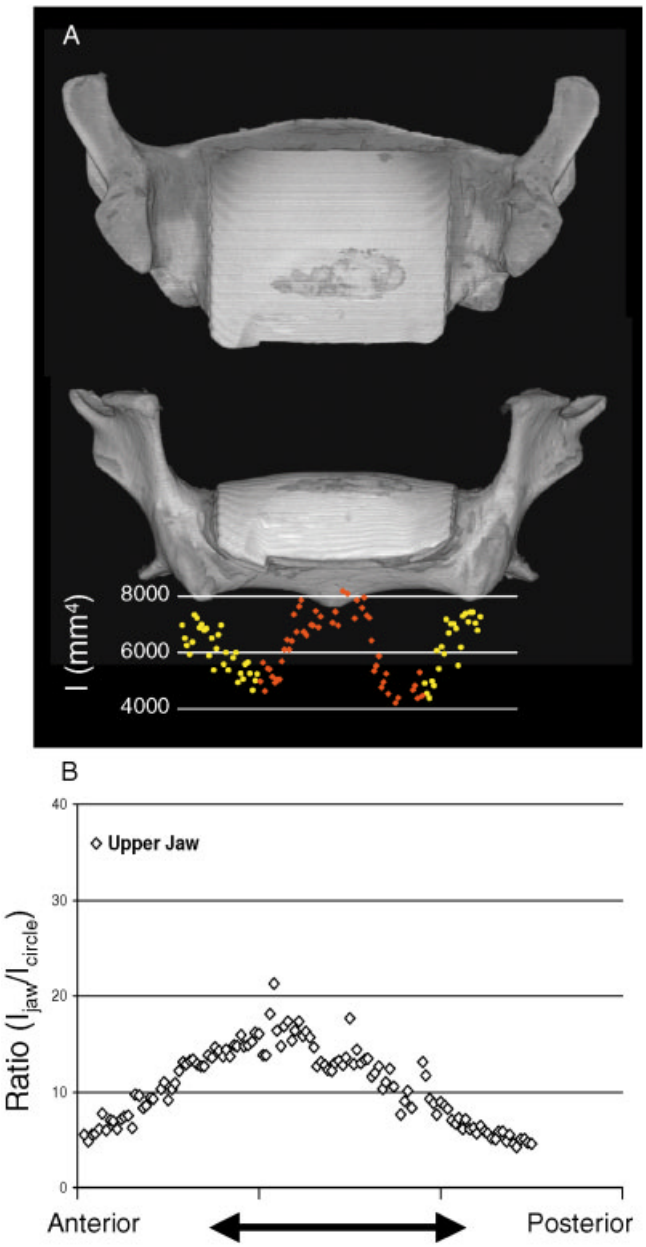

Fig. 7. Ventral (top) and anterior (bottom) view of a 3D reconstruction from a CT scan of a spotted eagle ray (*Aetobatus narinari*) upper jaw. The upper graph is the second moment of area of the cross section of the jaws. The red symbols represent sections that, according to tooth wear patterns, are engaged in crushing hard prey. The bottom graph is a dimensionless measure of cross sectional shape — the ratio of the second moment of area of the jaw cross section to the second moment of area of a circle with the same first moment of area. For both graphs the x-axis value of each point is the level at which the cross section is taken.

both the upper and the lower jaw a single skeletal element. The second moment of area analysis suggests that the stiffest region is the central area of the jaw, where crushing takes place (Fig. 7B). Comparing the second moment of area of the jaw to the second moment of a circular rod with the same mineralized area indicates that this region of the jaw makes better use of the mineralized tissue than more lateral areas (Fig. 7B). This calculation of second moment does not take into account the extra mineralization present in the form of reinforcing struts in the trabecular cartilage of both upper and lower jaws. Adding the second moment due to these struts, were it practical, would undoubtedly increase the value considerably, as radiographs indicate as much mineral is in the struts as is in the outer layers (Summers, 2000).

In contrast, the horn shark has a completely unmineralized, and therefore very flexible mental symphysis in both the upper and the lower jaw, and the jaw joint is very tight, with no soft tissue between the elements. Second moment analysis indicates that flexibility decreases from the tip of the jaw to the molariform teeth, and then continues increasing until the jaw joint. There is no suggestion of trabecular cartilage in the jaws, supporting the hypothesis that this particular adaptation to crushing hard prey is a unique synapomorphy of the myliobatid stingrays. The second moment of area indicates that the horn shark jaws are more flexible than those of the eagle ray, but this is due to the greater degree of mineralization in the eagle ray. The horn shark makes better use than the stingray of the mineralized tissue it has (Figs. 6, 7). In short, while the upper and lower jaws of the stingray form a single, central crushing unit, the horn shark has independent left and right sides, with crushing teeth spanning the middle third (in adults) of both sides, and while the horn shark jaws are not as heavily mineralized as those of the stingray, they have a more advantageous arrangement of the mineralization.

It is worth noting that although there are no studies of the hardness of the prey consumed by horn sharks and myliobatid stingrays there is some indication that the latter concentrates on harder prey. In one study, about 60% of the horn shark's diet was prey that required crushing and half of that total was the relatively poorly defended pelecypods (scallops), and the remainder was crabs. The rest of the prey could be digested without reduction between the molariform teeth, including univalve mollusks

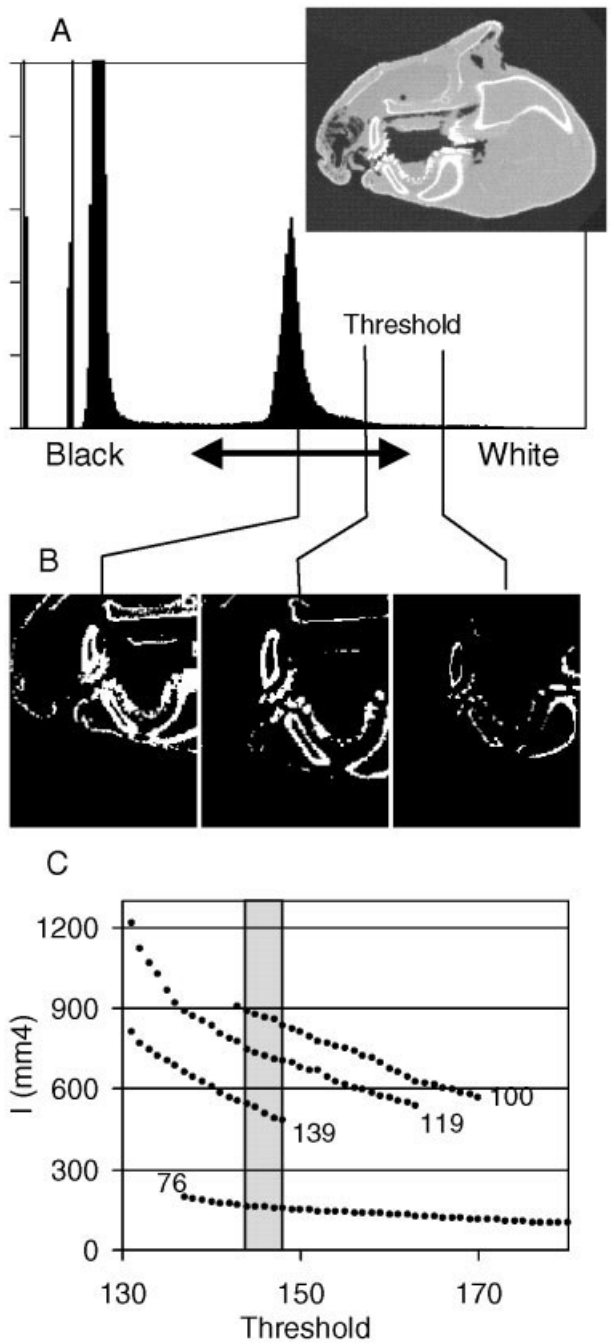

Fig. 8. **A:** Histogram of gray values (0–255) from the grayscale CT scan section (number 076) inset in the upper right. The various grays of the soft tissue and mineralized tissue make up the broad central peak. The peaks to the left represent the darker grays and black of the background. **B:** Binary bitmaps generated from the grayscale image inset in (**A**) by setting three different threshold values. Gray values equal to or below the threshold are interpreted as black, while values above threshold are white. The left image represents a threshold of 130, the center 150, and the right image 170. Only the central image reproduces the mineralization patterns that are clear from the grayscale image. **C:** The relationship between the image threshold and the calculated second moment (I) of area for four randomly chosen CT scan sections of the upper jaw of the adult horn shark (sections 76, 100, 119, and 136). There is a linear relationship between threshold and I. The mineralization pattern is reproduced well for these sections only over the relatively narrow range of threshold denoted by the gray shaded box.

(presumably sucked off of the substrate) and shrimp (Segura-Zarzosa et al., 1997). The eagle ray and cownose rays are reported to eat hard prey to the exclusion of all else, save the occasional, incidental ingestion of sea grass and epiphytes. Their diet consists nearly exclusively of bivalve mollusks, including hard clams and oysters, as well as decapod crustaceans (Gudger, 1914; Coles, 1915; Fowler, 1917). The rays reach a larger adult size than hornsharks, but are durophagous from birth, so we do not expect that the difference in diet is due purely to adult size. This apparent preference for somewhat softer prey on the part of the horn shark bears further investigation in light of our data that show the jaws to be less able to resist bending.

Ontogeny of Crushing

Although there are no ontogenetic studies of the diet of horn sharks, morphological evidence suggests that they probably do not start life as hard prey specialists. In the cownose ray, a specialist on hard prey from birth (Schwartz, 1967, 1989), the crushing dentition, trabecular cartilage, and hypertrophied muscles needed for durophagy are found in late stage embryos (Summers, 2000). The horn shark neonate has poorly mineralized molariform teeth and key regions of the jaws are also poorly mineralized. Were the teeth functional in crushing, we expect that the area under the teeth would be well mineralized, as would the deeply curved ventral insertion of the adductor muscles on Meckel's cartilage, yet both are barely radio-opaque. Instead, the jaw joint mineralizes very early in ontogeny; opposing surfaces are calcified even in a 10-mm-long cranium. In addition, the early mineralization of the hyoid elements suggests that even neonatal sharks are able to suction feed (Wu, 1994; for a discussion of the importance of these skeletal elements, see Wilga et al., 2000).

The 37-cm horn shark, an immature animal, has attained a degree of mineralization in the jaws and specialization of the teeth that indicate it could eat hard prey. This trend continues into adulthood, and the largest animal scanned has built up multiple layers of tesserae on the jaws (Fig. 2), an indication of high stress in that area (Dingerkus et al., 1991). We infer from the morphological data that these sharks are suction feeders throughout their life, concentrating on harder prey as adults. That the adults are powerful suction feeders is supported by Emonds' et al. (2001) documentation of the kinematics of horn sharks feeding on a variety of prey items.

CT Scanning

The CT scan is an expensive and equipment-intensive way to investigate hard tissue morphology. The question "Why not use a sharp knife?" is pertinent and should be answered before undertaking a scanning study. We chose to use CT in this study for three reasons. A primary reason was the ability of CT to produce digital, "virtual" sections along any line. This was instrumental in being able to gather the second moment of area data. There are physical serial sectioning techniques that may have worked, but they are time-consuming and do not have the advantage of sectioning perpendicular to a line through a particular skeletal element. The capabilities of the micro-source CT scanner allowed us to image the neonatal shark, with a cranium 10 mm in length with sections taken every 0.06 mm. Visualizing the mineralized skeleton of this animal would only have been possible through time-consuming histological sectioning or whole-mount clearing and staining. Horn sharks are particularly difficult to clear and stain because even as neonates their skin has a thorough covering of well-mineralized dermal denticles. This requires skinning the animal prior to clearing, a process that, in animals with thick, tough skin, tends to damage the underlying skeletal tissue. The third reason that we chose CT scanning for this study is that it allows the visualization of mineralized tissues in their natural positions (e.g., Summers, 2000; Maisano et al., 2003). Manual dissection and clearing and staining alter the soft tissues, making it difficult to assess the relative position of skeletal elements. In particular, the degree of separation between the rami of the jaws would have been very difficult to assess via dissection (Fig. 2).

CT scanning has two other advantages over a knife that should have general appeal. 1) Scanning is a completely noninvasive method for examining important or rare specimens. This did not obtain in our study, but is often an important consideration for curators and has led to "virtual" dissections of a variety of otherwise poorly studied species (Maisano et al., 2003). 2) The digital nature of scanning has the added virtue of producing an output that is readily placed in the public domain. All of our scanned material was available soon after scanning on the worldwide web at Digital Morphology, an NSF-sponsored digital library (www.digimorph.org), as a resource for researchers, teachers, and the general public. This is a very direct way to disseminate results, provide a public resource, and distribute important morphological data (Rowe et al., 1999; Tykoski et al., 2002).

Evolution of Durophagy

A diet of hard prey has evolved in the chimeras (Holocephali), the horn sharks, the bonnethead shark, and in the myliobatid stingrays, and it seems likely that there are as many mechanisms for crushing hard prey as there are lineages. Each has radically different jaw morphology than the other,

highly divergent tooth morphology, and probably specializes on hard prey to different degrees. The jaws of the chimera are narrow and deep, like those of the horn shark, but the symphysis is more heavily calcified and the teeth are fused into a pair of upper and lower plates. Their morphology indicates that chimaeras, like the stingrays, crush hard prey in the center of their jaws. The horn shark, as seen here and elsewhere, crush hard prey between molariform teeth closer to the jaw joint. The bonnethead shark, a small, coastal species of hammerhead shark, has strongly molariform teeth and makes swimming crabs (Callinectidae) a large part of its diet. There are several studies that have investigated the difficulty of crushing certain mollusks, but there are scant data on the particular prey items crushed by these four lineages. In order to understand the evolution of the crushing mechanism, we need to understand how the jaws perform in nature. This requires a concerted effort to determine the strength of the prey items commonly found in the diets of these animals. Without these data the strongest statement we can make is that each of the lineages has arrived at a different solution to the difficult problem of cracking hard prey.

ACKNOWLEDGMENTS

Ronald McConnaughey, P. McConnell, J.D. Dubick and Eddie Kisfaludi for generously supplying the materials used in this study; Steve Kajiura, Eliot Drucker, Justin Schaefer, and Marianne Porter read and improved earlier drafts.

LITERATURE CITED

Applegate SP. 1967. A survey of shark hard parts. In: Gilbert PW, Mathewson RF, Rall DP, editors. Sharks, skates and rays. Baltimore: Johns Hopkins Press. p 37–68.

Beer FP, Johnston ER Jr. 1977. Vector mechanics for engineers: statics and dynamics. New York: McGraw Hill.

Bleeker P. 1977. Atlas ichthyologique des Indes orientales néêrlandaises. Washington, DC: Smithsonian Institution.

Cifelli RL, Lipka TR, Schaff CR, Rowe TB. 1999. First Early Cretaceous mammal from the Eastern Seaboard of the United States. J Vertebr Paleontol 19:199–203.

Clark JM, Norell MA, Rowe T. 2002. Cranial anatomy of *Citipati osmolskae* (Theropoda, Oviraptorosauria), and a reinterpretation of the holotype of *Oviraptor philoceratops*. Am Mus Novit 3364:1–24.

Clement JG. 1992. Re-examination of fine structure of endoskeleal mineralization in chondrichthians: implications for growth, aging and calcium homeostasis. Aust J Mar Freshw Res 43: 157–181.

Coates MI, Sequeira EK. 2001. Early sharks and primitive gnathostome interrelationships. In: Ahlberg PE, editor. Major events in early vertebrate evolution. London: Taylor and Francis. p 241–262.

Coates MI, Sequeira SEK, Sansom IJ, Smith MM. 1998. Spines and tissues of ancient sharks. Nature 396:729–730.

Coles RJ. 1910. Observations on the habits and distribution of certain fishes taken on the coast of North Carolina. Bull Am Mus Nat Hist 28:338–341.

Coles RJ. 1915. Notes on the sharks and rays of Cape Lookout, N.C. Proc Bio Soc Wash 28:89–94.

Compagno LJV. 1984. Sharks of the world — an annotated and illustrated catalogue of shark species known to date. New York: United Nations FAO Guide.

Dingerkus G, Seret B, Guilbert E. 1991. Multiple prismatic calcium phosphate layers in the jaws of present-day sharks (Chondrichthyes; Selachii). Experientia 47:38–40.

Edmonds MA, Motta PJ, Hueter RE. 2001. Food capture kinematics of the suction feeding horn shark, *Heterodontus francisci*. Environ Biol Fishes 62:415–427.

Fierstine HL, Walters V. 1968. Studies in locomotion and anatomy of scombroid fishes. Los Angeles: Anderson, Ritchie & Simon.

Fowler HW. 1917. Notes on the fishes of New Jersey, Pennsylvania, and Maryland. Proc Acad Nat Sci Philadel 69.

Garman S. 1913. The Plagiostomia. Mem Mus Comp Zool 36:1–515.

Gudger EW. 1914. History of the spotted eagle ray, *Aëtobatus narinari,* together with a study of its external structures. Carnegie Inst Wash 183:241–323.

Gudger EW. 1941. The food and feeding habits of the whale shark, *Rhineodon typus*. J Elisha Mitchell Sci Soc 57:57–72.

Halstead LB. 1974. Vertebrate hard tissues. London: Wykeham Publications; distributed by Chapman & Hall.

Kemp NE, Westrin SK. 1979. Ultrastructure of calcified cartilage in the endoskeletal tissue of sharks. J Morphol 160:75–102.

Ketcham RA, Carlson WD. 2001. Acquisition, optimization and interpretation of X-ray computed tomographic imagery: applications to the geosciences. Comput Geosci 27:381–400.

Lund R, Grogan ED. 1997. Relationships of the chimaeriformes and the basal radiation of the Chondrichthyes. Rev Fish Biol Fish 7:65–123.

Maisano JA, Bell CJ, Gauthier J, Rowe T. 2003. The osteoderms and palpebral bones in *Lanthanotus borneensis* (Squamata: Anguimorpha). J Herpetol 36:678–682.

Nobiling G. 1977. Die Biomechanik des Keiferapparates beim Stierkopfhai (*Heterodontus portusjacksoni = Heterodontus philippi)*. Adv Anat Embryol Cell Biol 52.

Ørvig T. 1951. Histologic studies of Placoderm and fossil elasmobranchs. I. The endoskeleton, with remarks on the hard tissues of lower vertebrates in general. Arkiv For Zool 2:321–454.

Parker WK. 1879. On the structure and development of the skull in sharks and skates. Trans Zool Soc Lond 10:189–234.

Ridewood WG. 1921. On the calcification of the vertebral centra in sharks and rays. Philos Trans R Soc Lond 210:311–407.

Rowe T. 1996. Coevolution of the mammalian middle ear and neocortex. Science 273:651–654.

Rowe T, Brochu CA, Kishi K. 1999. Cranial morphology of alligator and phylogeny of Alligatoroidae. Soc Vertebr Paleontol Mem 6 J Vertebr Paleontol 19 (Supp) 1–100.

Rowe T, Kappelman J, Carlson WD, Ketcham RA, Denison C. 1997. High-resolution computed tomography: a breakthrough technology for earth scientists. Geotimes 42:23–27.

Schwartz FJ. 1967. Embryology and feeding behavior of the Atlantic cownose ray, *Rhinoptera bonasus*. Association of Island Marine Laboratories of the Caribbean (7th Meeting): 15.

Schwartz FJ. 1989. Feeding behavior of the cownose ray, *Rhinoptera bonasus* (family Myliobatidae). ASB Bull 36:66.

Segura-Zarzosa JC, Abitia-Cardenas LA, Galvan-Magana F. 1997. Observations on the feeding habits of the shark *Heterodontus francisci* Girard 1854 (Chondrichthyes: Heterodontidae), in San Ignacio Lagoon, Baja California Sur, Mexico. Ciencias Marinas 23:111–128.

Shirai S. 1996. Interrelationships of the living neoselachians (Chondrichthyes: Neoselechii). In: Stiassny MLJ, Parenti LR, Johnson GD, editors. Interrelationships of fishes. New York: Academic Press. p 9–34.

Smith BG. 1942. The heterodontid sharks: their natural history, and the external development of *Heterodontus japonicus* based on notes and drawings by Bashford Dean. In: Gudger EW, editor. The Bashford Dean memorial volume — archaic fishes. New York: American Museum of Natural History. p 651–769.

Smith MM, Hall BK. 1990. Development and evolutionary origins of vertebrate skeletogenic and odontogenic tissues. Biol Rev 65:277–373.

Summers AP. 2000. Stiffening the stingray skeleton — an investigation of durophagy in myliobatid stingrays (Chondrichthyes, Batoidea, Myliobatoidea). J Morphol 243:113–126.

Summers AP, Koob TJ, Brainerd EL. 1998. Stingray jaws strut their stuff. Nature 395:450–451.

Tykoski RS, Rowe T, Ketcham R, Colbert M. 2002. Calsoyasuchus valliceps, a new crocodyliform from the Early Jurassic Kayenta Formation of Arizona. J Vertebr Paleontol 22:593–611.

Wainwright SA, Biggs WD, Currey JD, Gosline JM. 1976. Mechanical design in organisms. Princeton, NJ: Princeton University Press.

Wilga CD, Motta PJ. 2000. Durophagy in sharks: feeding mechanics of the hammerhead *Sphyrna tiburo*. J Exp Biol 203:2781–2796.

Wilga CD, Wainwright PC, Motta PJ. 2000. Evolution of jaw depression mechanics in aquatic vertebrates: insights from Chondrichthyes. Biol J Linn Soc 71:165–185.

Wu EH. 1994. Kinematic analysis of jaw protrusion in orectolobiform sharks: a new mechanism for jaw protrusion in elasmobranchs. J Morphol 222:175–190.